NANO LETTERS

pubs.acs.org/NanoLett

Letter

Three-Dimensional Multiorbital Flat Band Models and Materials

Jingyi Duan, Chaoxi Cui, Minjun Wang, Wei Jiang,* and Yugui Yao*

Cite This: https://doi.org/10.1021/acs.nanolett.4c04527

Read Online

ACCESS | Metrics & More | Article Recommendations | Supporting Information

ABSTRACT: Flat band (FB) systems are essential for uncovering exotic quantum phenomena associated with strong electron correlations. Here we present a systematic theoretical framework for constructing multiorbital FB models and identifying feasible material candidates. This framework integrates group theory and crystallography into a symmetry-adapted tight-binding model incorporating lattice, site, and orbital degrees of freedom. Using this approach, we unveil a novel three-dimensional (3D) multiorbital FB model in the face-centered-cubic lattice, distinct from well-known single-orbital Lieb and kagome models. Critically, we identify numerous high-quality binary materials with ultraclean 3D FBs near the Fermi level. Furthermore, we explore diverse orbital bases within this model and extend our analysis to other cubic lattices with different space groups, broadening the scope for realizing 3D multiorbital FB systems. Our findings provide a foundational platform for exploring correlated physics in multiorbital FB systems and guiding the discovery of new quantum materials.

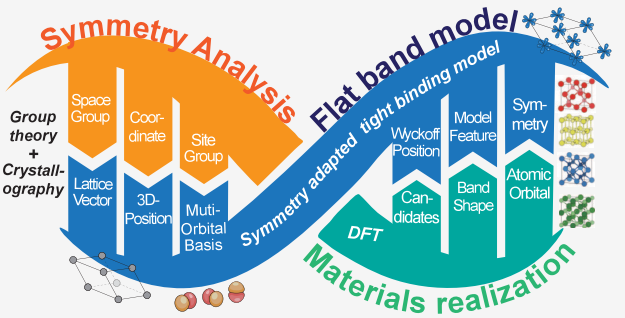

KEYWORDS: *flat band, group theory, crystallography, TB model, DFT calculation*

In the realm of condensed matter physics, electronic flat bands (FB) with quenched kinetic energy and amplified electron correlation are essential for the emergence of numerous exotic quantum phenomena.[1−9] Despite intensive investigations, the anticipated high-temperature superconductivity/fractional quantum anomalous Hall effect in FB systems remains elusive.[9−15] These uncertainties drive the search for more ideal intrinsic single-crystal FB materials,[16] especially focusing on the recently studied three-dimensional (3D) FB systems, which are anticipated to show enhanced superconductivity and novel quantum states.[17−19] However, the lack of ideal FB materials with high experimental feasibility and clean FB states near the Fermi level remains one of the biggest challenges, severely hindering progress in this field.

The study of FB can be traced back to 1986 in an attempt to achieve a "strictly localized state" in crystal lattices.[20] So far, the theoretical methods for FB study,[21−25] e.g., line-graph or split-graph theory,[21−23] the S-matrix method[26] in bipartite lattices, and the compact localized state (CLS) generator method,[27] are predominantly limited in single-orbital FB systems in low dimensions, such as typically studied Lieb and kagome lattices. Those limitations raise challenges for the experimental verification of predicted FB materials.[16,28−30] There are limited few studies of multiorbital FB in existing simple two-dimensional lattices,[31−36] such as the (p_x, p_y) hexagonal model,[31,32] the (p_x, p_y, $d_{x^2-y^2}$) square model,[35] etc., which have already demonstrated their complexity, presenting unprecedented challenges to the existing research methods for FB investigation. As the majority of real materials are 3D and multiorbital, a suitable methodology that can systematically integrate dimensionality and orbital degrees of freedom into FB systems is urgently needed.

In this paper, combining group theory, crystallography, and the symmetry-adapted tight-binding (TB) method with the construction of CLS, we introduce a systematic methodology to map out FB models considering all the aforementioned degrees of freedom. Our approach provides essential material information, such as space group (SG), Wyckoff position (WP), and point group (PG) information, to facilitate the search for realistic FB materials. This methodology not only significantly enriches the diversity of FB lattice models but also prepares them for the identification of feasible material candidates, especially those with multiple orbitals. To illustrate our method, we detail the construction of a novel 3D three-orbital FB model within the face-centered-cubic (FCC) lattice, which is fundamentally distinct from the conventionally studied single-orbital FB models like Lieb and kagome models, and the identification of a large family of high-quality FB materials featuring an ultraclean 3D FB near the Fermi level. We further demonstrate how such a framework can be applied to the other multiorbital FB systems.

Received: September 14, 2024
Revised: November 20, 2024
Accepted: November 21, 2024
Published: November 25, 2024

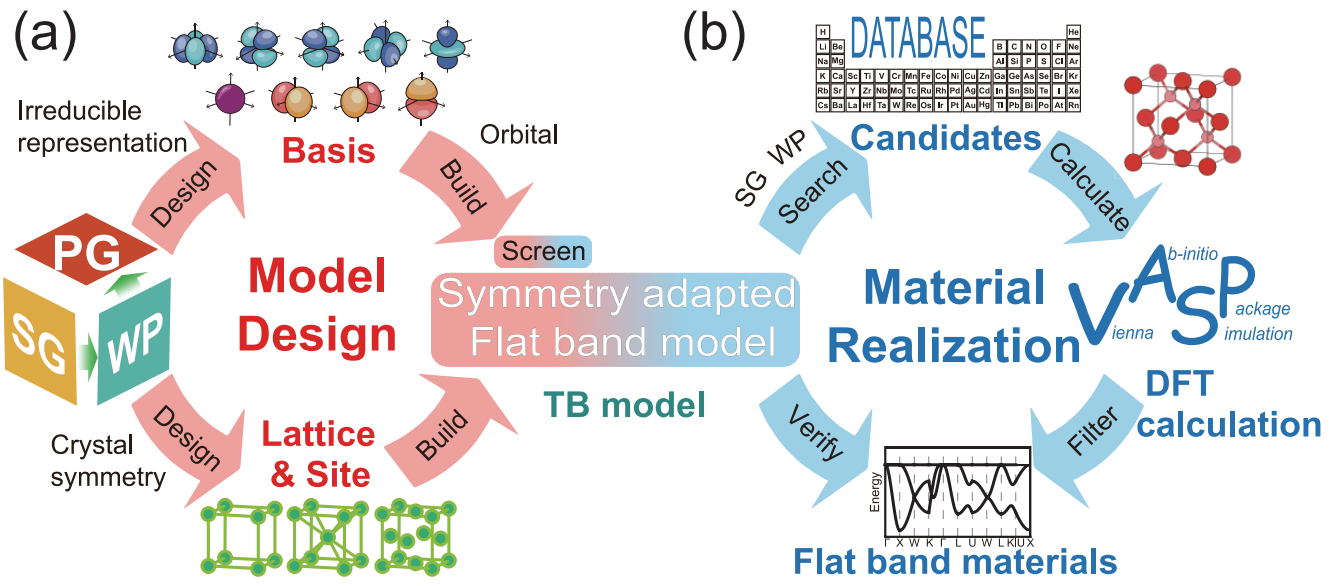

Figure 1. Theoretical framework for exploring multiorbital FB systems. The FB searching framework contains two modules. (a) The first module handles the FB model design based on symmetry-adapted TB model designing, building, and screening processes, which consider the lattice, site, and orbital degrees of freedom. SG, PG, and WP represent the space group, point group, and Wyckoff position, respectively. (b) The second module handles the material realization by treating the FB materials searching, calculating, filtering, and verification processes. It searches material candidates using the WP and SG information from the model design process, followed by high-throughput DFT calculations and FB material verification.

Symmetry-Adapted Flat Band Framework. Generally, the lattice geometry enforced destructive interference of electrons is acknowledged as the crucial ingredient for the development of FB materials.[37] However, the interplay between the Bravais lattice, site, and orbital symmetry that is known to be constrained by crystal symmetry in realistic materials has been seldom considered in previous studies. Such a deficiency inevitably leads to a significant mismatch between the proposed lattice models and realistic materials. Here, we present a symmetry-adapted FB framework rooted in group theory and crystallography (shown in Figure 1), which seamlessly incorporates both the FB model design [Figure 1(a)] and material realization [Figure 1(b)] modules.

As illustrated in Figure 1(a), the FB model design module starts from crystallography analysis that incorporates SG, WP, and PG. SGs with restricted symmetries within crystal systems impose limitations on the corresponding Bravais lattice. WPs, representing subgroups of positions that have the same site symmetry operation for each SG, provide essential coordinate information about sites. Moreover, the PG of the site symmetry of WPs constrains the potential orbital bases and their irreducible representations (irrep). With the lattice, coordinates of the WPs (sites), and the corresponding symmetry-constrained orbital bases (basis), we are able to construct a symmetry-adapted TB model.[38] Further, we employ high-throughput TB band structure calculations to explore the parameter space created by different hopping parameters. This enables us to thoroughly investigate each combination of SG, WP, and PG to facilitate the search for more realistic FB models.

The material realization module can be expedited accordingly, as described in Figure 1(b). Building upon the symmetry-adapted FB model, the information from PG and WPs is utilized to guide the preliminary selection and/or design of material candidates[39,40] from various material databases.[41,42] Essential information on the material candidates is collected for high-throughput first-principles calculations (more details in Supporting Information (SI) S1[43]). The calculated band structure, fitted Hamiltonian, and realistic orbital contributions of the material candidates are cross checked with the initial FB model to verify the material realization. To showcase the feasibility of this framework, we illustrate our discovery of a novel 3D multiorbital FB model in the FCC lattice, along with its material realization in a large family of binary compounds. We note that such an intriguing FB model has also been reported recently[44] during the review of our work; however, we focus more on the symmetry-adapted flat band framework. We will show that this framework can be more general and can be extended beyond the FCC lattice model.

3D Multiorbital FB Models. In contrast to extensively studied FB systems in one and two dimensions, where a variety of lattices have been discovered (S2A and S2B in the SI[43]), the exploration of 3D FB systems remains considerably limited (S2C in SI[43]). The most studied 3D FB systems, such as the 3D kagome (pyrochlore)[45] and 3D Lieb (perovskite)[46] lattices, are primarily derived from dimensional extension from their 2D counterparts.[21,22] Recent experimental observations of 3D flat bands in pyrochlore crystals,[18] along with theoretical predictions of their unique topological and superconducting properties,[19,44] have reignited interest in the field. Given that most existing 3D FB lattice models use a single-orbital basis while real materials are inherently multiorbital, it is crucial to extend FB research into the multiorbital domain.

We initiated our study from one of the most fundamental cubic lattices, i.e., the FCC lattice with SG $Fm\bar{3}m$ (SG-225), as illustrated in Figure 2a, considering one single site (WP-4*a*) in each primitive cell, which belongs to the PG-O_h with the site symmetry $m\bar{3}m$. The site symmetry analysis can produce the irrep for different orbital bases, e.g., the irrep for *p* orbitals

https://doi.org/10.1021/acs.nanolett.4c04527
Nano Lett. XXXX, XXX, XXX−XXX

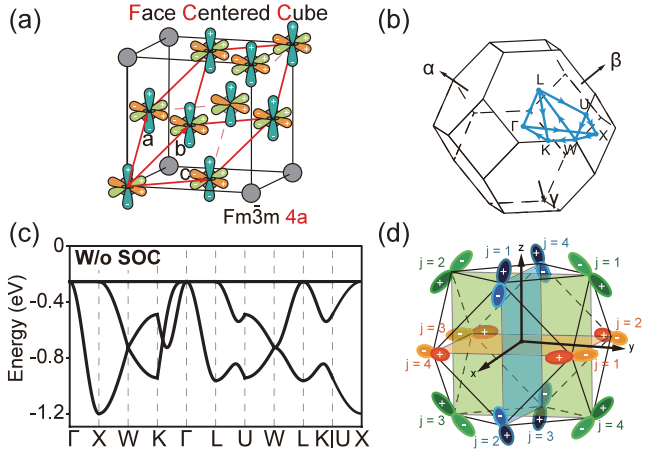

Figure 2. Multiorbital 3D FB in the FCC lattice. (a) Crystal structure of the FCC lattice with the conventional and the primitive cell highlighted by black and red lines, respectively. Each site is occupied by three degenerate p_x, p_y, and p_z orbitals. (b) Depiction of the first Brillouin zone of the FCC lattice, accompanied by its high-symmetry k points. (c) Band structure of the p_x, p_y, p_z three-orbital FCC lattice without SOC ($-t_1 = t_2 = t_3 = 0.06$). (d) The compact localized state associated with the FB.

(T_{1u}) and d orbitals (T_{2g} and E_g), which provide the essential information to describe the orbital degree of freedom. Using T_{1u} as an example, i.e., triply degenerate p_x, p_y, and p_z orbitals illustrated in Figure 2a, after applying the symmetry-adapted TB model based on the group symmetry analysis (MagneticTB),[38] we obtain a multiorbital TB model for the FCC lattice.

The Hamiltonian considering only the nearest-neighbor (NN) interaction is described as

$$\begin{aligned}\mathcal{H}_{\mathrm{FCC}} &= \sum_{\alpha,R} \epsilon_\alpha a_\alpha^{R\dagger} a_\alpha^R + t_1 \sum_{r_{\langle\alpha\rangle}} \sum_{\alpha,R} a_\alpha^{R+r_{\langle\alpha\rangle}\dagger} a_\alpha^R \\ &+ t_2 \sum_{r_{\langle\gamma\rangle}}^{\gamma\neq\alpha\neq\beta} \sum_{\alpha,R} \eta_{r_{\langle\gamma\rangle}} a_\beta^{R+r_{\langle\gamma\rangle}\dagger} a_\alpha^R \\ &+ t_3 \sum_{r_{\langle\beta\rangle}}^{\beta\neq\alpha} \sum_{\alpha,R} a_\alpha^{R+r_{\langle\beta\rangle}\dagger} a_\alpha^R, \end{aligned} \tag{1}$$

in which $\{\alpha, \beta, \gamma\} = \{x, y, z\}$. R represents the atomic position, and $r_{\langle\alpha\rangle}$ denotes the position vector for NNs in the plane perpendicular to the p_α orbital. $\eta_{r_{\langle\gamma\rangle}} = \pm 1$ for different hopping directions (SI Table 1.[43]). $t_{1,2,3}$ represent the hopping parameter between the same out-of-plane orbitals, the hopping between different in-plane orbitals, and the hopping between the same in-plane orbitals within the corresponding plane, respectively (further details in S3A in SI[43]). Through high-throughput TB band structure calculations of various combinations of $t_{1,2,3}$ (more details in SI S3A[43]), an FB emerges across the entire 3D Brillouin zone [Figure 2(b)] when $-t_1 = t_2 = t_3$, as shown in Figure 2(c). The change of t_1, t_2, and t_3 values will introduce dispersion to the flat band, which scales with the difference between these t values (see S3A in SI[43] for more details). We note that for realistic materials, such hopping amplitudes will strongly depend on the local environment and element species, which requires detailed band structure calculation.

To better understand the nature of the 3D FB, we calculated the corresponding CLS (S3B in SI[43]) based on the Hamiltonian in eq 1. The CLS takes the form

$$|\psi^\alpha\rangle = \sum_{j=1}^{4} (-1)^j \{-\sin\theta |P_\beta^j\rangle + \cos\theta |P_\gamma^j\rangle\} \varepsilon_{\alpha\beta\gamma} \tag{2}$$

where $j = 1-4$, $\theta = \frac{\pi}{2}j - \frac{\pi}{4}$, representing the four vertices of the α-square plane, as shown in Figure 2(d), $\varepsilon_{\alpha\beta\gamma}$ denotes the Levi–Civita symbol, and P_γ^j denotes the jth p_γ orbital. As shown in Figure 2(d), the CLS of the 3D FB is localized at the 12 NN sites from the center position. These 12 sites can be categorized into three distinct groups, corresponding to xy, xz, and yz planes, represented by orange, blue, and green colors, respectively. These orbitals collectively form a cuboctahedron, encasing the CLS within a 3D cluster. We note that the CLS exhibits odd behavior under spatial inversion, while the eigenvalues of C_{3-111}, C_{4i}, and C_{2i} ($i = x, y$, and z) rotational symmetry operations are +1, −1, and +1, respectively. This CLS with high symmetry effectively prevents any external electron hopping through destructive interference across the entire 3D space. Such unique configuration of CLS is inherently rooted in its multiorbital nature, fundamentally distinguishing it from previous single-orbital FB systems.[27,47] We further studied the spin–orbit coupling effect of the model, which leads to gap opening and dispersion of the flat band and also intriguing topological properties (S3D-F in SI[43]).

Considering variations in structural symmetry of realistic materials, we explored the FB model in four additional SGs beyond the $Fm\bar{3}m$ (SG-225) with the cubic structure that supports WP-4a, namely, $F23$ (SG-196), $Fm\bar{3}$ (SG-202), $F432$ (SG-209), and $F\bar{4}3m$ (SG-216). Despite different site symmetries, all these structures support perfect 3D multiorbital FBs, identical to that in the ideal FCC lattice (S3C in SI[43]).

Material Realization. With the FB models, material realization remains a paramount challenge in the study of FB physics. This work is dedicated to contributing significantly to this aspect, focusing on identifying materials with a clean band structure and high experimental feasibility. Using the SG and WP information gathered from the FB model as searching criteria, we explored various materials databases,[41,42] from which we started the material search, particularly focusing on the binary compounds. Due to the reduction of symmetry of these four SGs, additional modulation parameters are introduced to guarantee the existence of a flat band. This strategic approach led to the discovery of three simple families of materials in SG-225 with WP-4a that align perfectly with the model. These are summarized in Figure 3(a), comprising rock salt (yellow, S4A in SI[43]), fluorite (blue, S4B in SI[43]), and cubic DO_3 structures (green, S4C in SI[43]). In addition, we disclosed another similar system with the zincblende structure (red, S4D in SI[43]) in SG-216 with WP-4a that also satisfies the multiorbital FCC FB model. For each family of materials, we mapped the binary elemental compositions onto the periodic table, employing corresponding color codes for clarity [Figure 3(a)]. These can be classified as nonmagnetic MX ($M^{i+}X^{i-}$, $i = 1-3$), M_2X ($M_2^{i+}X^{2i-}$, $i = 1, 2$), and $M_3^{1+}X^{3-}$ (S4 in SI). M^{i+} with $i = 1-3$ corresponds to the group IA, IIA, and IIIB cationic elements, while X^{i-} with $i = 1-4$ corresponds to the group VIIA to IVA anionic elements, which ensures the closed-shell configuration for each component. We note that there is not a strict numerical threshold for bandwidth that universally

https://doi.org/10.1021/acs.nanolett.4c04527
Nano Lett. XXXX, XXX, XXX−XXX

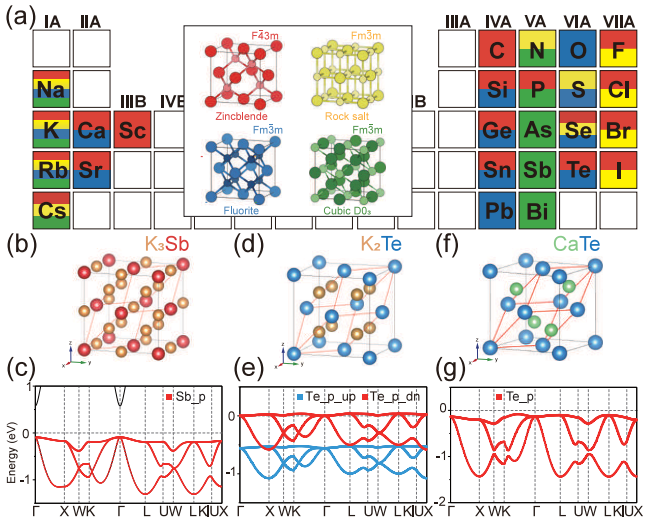

Figure 3. An overview of binary material candidates with 3D multiorbital FB. (a) Binary materials that align with the three-orbital FCC model in four families of distinct materials, i.e., zincblende (red, SG-216), rock salt (yellow, SG-225), fluorite (blue, SG-225), and cubic $D0_3$ structure (green, SG-225). The color markings on the periodic table are the same as those for crystal structures. The selection of a pair of cationic (M) and anionic element (X) from the same color leads to a material with the corresponding lattice. (b) Representative nonmagnetic FB material K_3Sb in SG-225 with the cubic DO_3 structure and (c) the orbital-projected band structure without SOC. (d, e) Same as (b),(c) for a magnetic FB material, doped K_2Te with one hole, in SG-225 with fluorite structure. (f, g) Same as (b),(c) for inversion symmetry broken FB material, CaTe in SG-216 with zincblende structure.

defines a band as "flat", due to the intrinsically distinct bandwidth of different atom orbitals. As a band is often considered flat when its bandwidth is much smaller than the bandwidths of neighboring bands, we chose this as one of the criteria in this study to select high-quality flat band materials.

Such a closed-shell configuration plays a critical role in generating ultraclean FB systems with precisely three bands as the model aligning right below the Fermi level. Additionally, ideal ferromagnetic systems can be easily realized through hole doping of the FB, such as in compounds $M^{i+}X^{(i+1)-}$ with $i = 1-3$ and $M^{1+}X^{3-}$ (S4 in SI[43]). After performing high-throughput first-principles calculations and comparing results to the model, we showcased 74 high-quality FB materials, 30 of which have been synthesized (Table 2 in S4 of SI[43]). We note that beyond the materials presented here, numerous material systems could potentially satisfy the multiorbital FB model. These include binary compounds with transition metal elements, as well as ternary and quaternary compounds from the Heusler alloy family and others, which merit further exploration. Below, we detail three representative materials. We note that potentially due to the reduced symmetry, the available material candidates for the other three SGs, i.e., SG-196, 202, and 209, are very rare (38 materials in total in the Materials Project database), and no ideal FB material is found.

The nonmagnetic material, K_3Sb, in cubic DO_3 structure (SG-225) is shown in Figure 3(b), where Sb occupies the WP-4*a* site while K occupies both WP-4*b* and 8*c* sites. The band structure of the K_3Sb without SOC around the Fermi level closely resembles the 3D multiorbital FB in the FCC lattice, with only minor dispersion of the FB due to unavoidable long-range interactions, as shown in Figure 3(c). Further, we utilized the Wannier90 package[48,49] to fit these bands and extract the corresponding Hamiltonian, which is confirmed to be identical to the FB model. When analyzing different compounds in this family, we also discovered multiple interesting topological states associated with the 3D FB that are worth studying (S5 in SI[43]).

Generally, the partial filling of the FB is known to yield strong ferromagnetism,[50,51] which could lead to various intriguing quantum phenomena, especially for 3D FB systems.[19] To demonstrate this point, we calculated doped K_2Te in a fluorite structure (SG-225) with one hole, where Te and K occupy the WP-4*a* and 8*c* sites, respectively [Figure 3(d)]. While not considering SOC, the double-degenerate bands experience a large spin splitting with the FB of one spin channel located right at the Fermi level, as shown in Figure 3(e). When SOC is included, the system becomes a magnetic Weyl semimetal (S5 in SI[43]). We note there are multiple intrinsically magnetic material systems, such as ScGe and KS, characterized by the unbalanced charge between the cation and anion (S4 in SI[43]). These exhibit features similar to those of hole-doped K_2Te and await further exploration.

Additionally, materials with the zincblende structure in SG-216 ($F\bar{4}3m$) could also host a similar band structure. The crystal structure of the representative material, CaTe, is shown in Figure 3(f), with Ca and Te occupying the WP-4*a* and WP-

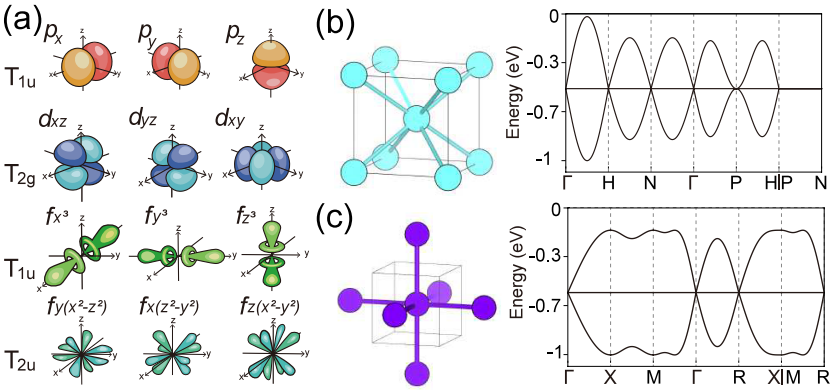

Figure 4. Extensions of the 3D multiorbital FB model. (a) Different orbital basis sets are explored: I. $\{p_x, p_y, p_z\}$, II. $\{d_{xy}, d_{yz}, d_{xz}\}$, III. $\{f_{x^3} f_{y^3} f_{z^3}\}$, IV. $\{f_{x(z^2-y^2)}, f_{y(z^2-x^2)}, f_{z(x^2-y^2)}\}$, which all yield the 3D FB. (b) The body-centered-cubic lattice and its corresponding FB in the three *p*-orbital TB model. (c) Same as (B) for the simple cubic lattice.

https://doi.org/10.1021/acs.nanolett.4c04527
Nano Lett. XXXX, XXX, XXX−XXX

4*c* sites, respectively. Similar to SG-225 compounds, the band structure without SOC shows the same features as the FB model [Figure 3(g)]. Note that due to the inversion symmetry breaking, extra band splitting is observed in *W*, *X* points and the Γ to *L* path.

General Multiorbital FB Systems. The 3D multiorbital FB model described so far is based on three degenerate *p* orbital bases [Figure 4(a)]. From the site symmetry analysis, similar triple degeneracy could extend to other orbitals, such as T_{2g} for *d* orbitals $\{d_{xy}, d_{yz}, d_{xz}\}$ and $T_{1u}\{f_{x^3}f_{y^3}f_{z^3}\}$ and $T_{2u}\{f_{x(z^2-y^2)}, f_{y(z^2-x^2)}, f_{z(x^2-y^2)}\}$ for *f* orbitals, as shown in Figure 4(a). Upon the integration of these orbital sets into our model, interestingly, we find that each set is capable of realizing FB similar to that illustrated in Figure 2(c). Further analysis of the corresponding TB model Hamiltonian and CLS can be found in S6 of SI.[43] These results affirm that the model's implementation transcends elemental constraints and is adaptable to a diverse range of real materials, where transition metal, lanthanide, and actinide elements constitute the lattice sites.

We further extended our study beyond the FCC lattice to include the other two cubic lattices, i.e., the body-centered-cubic (BCC) and the simple cubic (SC) lattices, as presented in Figure 4(b) and 4(c), respectively. The band structure of the BCC lattice with *I*432 (SG-211), WP-2*a*, and $\{p_x, p_y,$ and $p_z\}$ orbital bases is shown in Figure 4(b), which displays one FB in the middle of three bands with triple degeneracy along the high-symmetry *k*-path *P*−*N* (S7A and S7B of SI[43]). Similarly, the SC lattice model with *P*23 (SG-195), WP-1*a*, and $\{p_x, p_y, p_z\}$ orbital bases can also host a 3D multiorbital FB, as shown in Figure 4(c) (S7C and S7D in SI[43]).

To summarize, we propose a novel framework for the development of FB systems, focusing on both model design and material realization. By combining the group theory and crystallography analysis, notably leveraging insights from space group, point group, and Wyckoff positions, we are able to efficiently integrate lattice, site, and orbital degrees of freedom for the exploration of novel 3D multiorbital FBs. More importantly, this approach is fundamentally aligned with the properties of real materials, distinguishing our work from previous studies and greatly simplifying the practical application of these models to realistic materials.

We demonstrated its successful application in designing novel 3D three-orbital FB models in the FCC lattice, distinct from traditional low-dimensional single-orbital FB systems like Lieb and kagome lattices. We also identified numerous high-quality material candidates in binary compounds exhibiting ultraclean FB states near the Fermi level. Further, we showcased the versatility of this method by extending it to other cubic lattices with varying space groups and orbital bases, all of which feature intriguing 3D FBs. Additionally, the model exhibits several intriguing topological features, providing a novel playground for deeper exploration of this field.

In multiple orbital flat band systems, several unique physical phenomena and properties could be expected compared to single-orbital flat band systems due to the increased degrees of freedom and possible interactions between orbitals. For example, with multiple orbitals involved, electron−electron interactions become more complex, potentially leading to stronger correlation effects. The pairing mechanisms for superconductivity can also become more exotic with potentially unconventional pairing symmetries due to multiple orbitals. We anticipate that this study will unlock new insights into multiorbital correlated quantum phenomena in FB systems, facilitating further breakthroughs and applications.

■ ASSOCIATED CONTENT

Supporting Information

The Supporting Information is available free of charge at https://pubs.acs.org/doi/10.1021/acs.nanolett.4c04527.

(S1) Details of the methods, (S2) collection of FB lattice models, (S3) details of the 3D multiorbital FB model, (S4) representative FB materials, (S5) representative topological materials, (S6) 3D multiorbital FB models with different orbitals, (S7) FB models in other cubic lattices, and supporting tables and figures (PDF)

■ AUTHOR INFORMATION

Corresponding Authors

Wei Jiang − *Centre for Quantum Physics, Key Laboratory of Advanced Optoelectronic Quantum Architecture and Measurement (MOE), and Beijing Key Lab of Nanophotonics and Ultrafine Optoelectronic Systems, School of Physics, Beijing Institute of Technology, Beijing 100081, China*; orcid.org/0000-0001-6167-1156; Email: wjiang@bit.edu.cn

Yugui Yao − *Centre for Quantum Physics, Key Laboratory of Advanced Optoelectronic Quantum Architecture and Measurement (MOE), and Beijing Key Lab of Nanophotonics and Ultrafine Optoelectronic Systems, School of Physics, Beijing Institute of Technology, Beijing 100081, China*; orcid.org/0000-0003-3544-3787; Email: ygyao@bit.edu.cn

Authors

Jingyi Duan − *Centre for Quantum Physics, Key Laboratory of Advanced Optoelectronic Quantum Architecture and Measurement (MOE), and Beijing Key Lab of Nanophotonics and Ultrafine Optoelectronic Systems, School of Physics, Beijing Institute of Technology, Beijing 100081, China*

Chaoxi Cui − *Centre for Quantum Physics, Key Laboratory of Advanced Optoelectronic Quantum Architecture and Measurement (MOE), and Beijing Key Lab of Nanophotonics and Ultrafine Optoelectronic Systems, School of Physics, Beijing Institute of Technology, Beijing 100081, China*

Minjun Wang − *Centre for Quantum Physics, Key Laboratory of Advanced Optoelectronic Quantum Architecture and Measurement (MOE), and Beijing Key Lab of Nanophotonics and Ultrafine Optoelectronic Systems, School of Physics, Beijing Institute of Technology, Beijing 100081, China*

Complete contact information is available at: https://pubs.acs.org/10.1021/acs.nanolett.4c04527

Notes

The authors declare no competing financial interest.

■ ACKNOWLEDGMENTS

We acknowledge Yu-Xuan Li for helpful discussions. The research is supported by the National Key R&D Program of China (Grant Nos. 2020YFA0308800 and 2022YFA1403500) and the NSF of China (Grants Nos. 12204037, 12234003, and

12321004.). W.J. thanks the support from the Beijing Institute of Technology Research Fund Program for Young Scholars.

REFERENCES

(1) Neupert, T.; Santos, L.; Chamon, C.; Mudry, C. Fractional quantum Hall states at zero magnetic field. *Phys. Rev. Lett.* **2011**, *106*, 236804.

(2) Liu, Z.; Liu, F.; Wu, Y.-S. Exotic electronic states in the world of flat bands: From theory to material. *Chin. Phys. B* **2014**, *23*, 077308.

(3) Cao, Y.; Fatemi, V.; Demir, A.; Fang, S.; Tomarken, S. L.; Luo, J. Y.; Sanchez-Yamagishi, J. D.; Watanabe, K.; Taniguchi, T.; Kaxiras, E.; et al. Correlated insulator behaviour at half-filling in magic-angle graphene superlattices. *Nature* **2018**, *556*, 80−84.

(4) Hu, X.; Hyart, T.; Pikulin, D. I.; Rossi, E. Geometric and conventional contribution to the superfluid weight in twisted bilayer graphene. *Phys. Rev. Lett.* **2019**, *123*, 237002.

(5) Cao, Y.; Rodan-Legrain, D.; Rubies-Bigorda, O.; Park, J. M.; Watanabe, K.; Taniguchi, T.; Jarillo-Herrero, P. Tunable correlated states and spin-polarized phases in twisted bilayer-bilayer graphene. *Nature* **2020**, *583*, 215−220.

(6) Xie, F.; Song, Z.; Lian, B.; Bernevig, B. A. Topology-bounded superfluid weight in twisted bilayer graphene. *Phys. Rev. Lett.* **2020**, *124*, 167002.

(7) Törmä, P.; Peotta, S.; Bernevig, B. A. Superconductivity, superfluidity and quantum geometry in twisted multilayer systems. *Nat. Rev. Phys.* **2022**, *4*, 528−542.

(8) Herzog-Arbeitman, J.; Peri, V.; Schindler, F.; Huber, S. D.; Bernevig, B. A. Superfluid weight bounds from symmetry and quantum geometry in flat bands. *Phys. Rev. Lett.* **2022**, *128*, 087002.

(9) Cai, J.; Anderson, E.; Wang, C.; Zhang, X.; Liu, X.; Holtzmann, W.; Zhang, Y.; Fan, F.; Taniguchi, T.; Watanabe, K.; et al. Signatures of fractional quantum anomalous Hall states in twisted $MoTe_2$. *Nature* **2023**, *622*, 63−68.

(10) Tarnopolsky, G.; Kruchkov, A. J.; Vishwanath, A. Origin of magic angles in twisted bilayer graphene. *Phys. Rev. Lett.* **2019**, *122*, 106405.

(11) Lisi, S.; Lu, X.; Benschop, T.; de Jong, T. A.; Stepanov, P.; Duran, J. R.; Margot, F.; Cucchi, I.; Cappelli, E.; Hunter, A.; et al. Observation of flat bands in twisted bilayer graphene. *Nat. Phys.* **2021**, *17*, 189−193.

(12) Wu, S.; Zhang, Z.; Watanabe, K.; Taniguchi, T.; Andrei, E. Y. Chern insulators, van Hove singularities and topological flat bands in magic-angle twisted bilayer graphene. *Nat. Mater.* **2021**, *20*, 488−494.

(13) Cao, Y.; Fatemi, V.; Fang, S.; Watanabe, K.; Taniguchi, T.; Kaxiras, E.; Jarillo-Herrero, P. Unconventional superconductivity in magic-angle graphene superlattices. *Nature* **2018**, *556*, 43−50.

(14) Zeng, Y.; Xia, Z.; Kang, K.; Zhu, J.; Knüppel, P.; Vaswani, C.; Watanabe, K.; Taniguchi, T.; Mak, K. F.; Shan, J. Thermodynamic evidence of fractional Chern insulator in moiré MoTe2. *Nature* **2023**, *622*, 69−73.

(15) Wang, C.; Zhang, X.-W.; Liu, X.; He, Y.; Xu, X.; Ran, Y.; Cao, T.; Xiao, D. Fractional Chern insulator in twisted bilayer MoTe 2. *Phys. Rev. Lett.* **2024**, *132*, 036501.

(16) Regnault, N.; Xu, Y.; Li, M.-R.; Ma, D.-S.; Jovanovic, M.; Yazdani, A.; Parkin, S. S.; Felser, C.; Schoop, L. M.; Ong, N. P.; et al. Catalogue of flat-band stoichiometric materials. *Nature* **2022**, *603*, 824−828.

(17) Lau, A.; Hyart, T.; Autieri, C.; Chen, A.; Pikulin, D. I. Designing Three-Dimensional Flat Bands in Nodal-Line Semimetals. *Phys. Rev. X* **2021**, *11*, 031017.

(18) Wakefield, J. P.; Kang, M.; Neves, P. M.; Oh, D.; Fang, S.; McTigue, R.; Frank Zhao, S.; Lamichhane, T. N.; Chen, A.; Lee, S.; et al. Three-dimensional flat bands in pyrochlore metal $CaNi_2$. *Nature* **2023**, *623*, 301−306.

(19) Jiang, W.; De Sousa, D. J.; Wang, J.-P.; Low, T. Giant anomalous Hall effect due to double-degenerate quasiflat bands. *Phys. Rev. Lett.* **2021**, *126*, 106601.

(20) Sutherland, B. Localization of electronic wave functions due to local topology. *Phys. Rev. B* **1986**, *34*, 5208.

(21) Lieb, E. H. Two theorems on the Hubbard model. *Phys. Rev. Lett.* **1989**, *62*, 1201.

(22) Mielke, A. Ferromagnetic ground states for the Hubbard model on line graphs. *J. Phys. A* **1991**, *24*, L73.

(23) Chiu, C. S.; Ma, D.-S.; Song, Z.-D.; Bernevig, B. A.; Houck, A. A. Fragile topology in line-graph lattices with two, three, or four gapped flat bands. *Phys. Rev. Res.* **2020**, *2*, 043414.

(24) Ma, D.-S.; Xu, Y.; Chiu, C. S.; Regnault, N.; Houck, A. A.; Song, Z.; Bernevig, B. A. Spin-orbit-induced topological flat bands in line and split graphs of bipartite lattices. *Phys. Rev. Lett.* **2020**, *125*, 266403.

(25) Maimaiti, W.; Andreanov, A.; Flach, S. Flat-band generator in two dimensions. *Phys. Rev. B* **2021**, *103*, 165116.

(26) Călugăru, D.; Chew, A.; Elcoro, L.; Xu, Y.; Regnault, N.; Song, Z.-D.; Bernevig, B. A. General construction and topological classification of crystalline flat bands. *Nat. Phys.* **2022**, *18*, 185−189.

(27) Maimaiti, W.; Andreanov, A.; Park, H. C.; Gendelman, O.; Flach, S. Compact localized states and flat-band generators in one dimension. *Phys. Rev. B* **2017**, *95*, 115135.

(28) Liu, H.; Meng, S.; Liu, F. Screening two-dimensional materials with topological flat bands. *Phys. Rev. Mater.* **2021**, *5*, 084203.

(29) Duan, J.; Ma, D.-S.; Zhang, R.-W.; Jiang, W.; Zhang, Z.; Cui, C.; Yu, Z.-M.; Yao, Y. Cataloging High-Quality Two-Dimensional van der Waals Materials with Flat Bands. *Adv. Funct. Mater.* **2024**, *34*, 2313067.

(30) Neves, P. M.; Wakefield, J. P.; Fang, S.; Nguyen, H.; Ye, L.; Checkelsky, J. G. Crystal net catalog of model flat band materials. *npj Comput. Mater.* **2024**, *10*, 39.

(31) Wu, C.; Bergman, D.; Balents, L.; Das Sarma, S. Flat bands and Wigner crystallization in the honeycomb optical lattice. *Phys. Rev. Lett.* **2007**, *99*, 070401.

(32) Liu, C.-C.; Guan, S.; Song, Z.; Yang, S. A.; Yang, J.; Yao, Y. Low-energy effective Hamiltonian for giant-gap quantum spin Hall insulators in honeycomb X-hydride/halide (X= N−Bi) monolayers. *Phys. Rev. B* **2014**, *90*, 085431.

(33) Liu, H.; Sethi, G.; Meng, S.; Liu, F. Orbital design of flat bands in non-line-graph lattices via line-graph wave functions. *Phys. Rev. B* **2022**, *105*, 085128.

(34) Ni, X.; Li, H.; Liu, F.; Brédas, J.-L. Engineering of flat bands and Dirac bands in two-dimensional covalent organic frameworks (COFs): relationships among molecular orbital symmetry, lattice symmetry, and electronic-structure characteristics. *Mater. Horiz.* **2022**, *9*, 88−98.

(35) Sun, K.; Gu, Z.; Katsura, H.; Das Sarma, S. Nearly flatbands with nontrivial topology. *Phys. Rev. Lett.* **2011**, *106*, 236803.

(36) Xu, S.; Wu, C. Orbital-active Dirac materials from the symmetry principle. *Quantum Font* **2022**, *1*, 24.

(37) Leykam, D.; Andreanov, A.; Flach, S. Artificial flat band systems: from lattice models to experiments. *Adv. Phys. X* **2018**, *3*, 1473052.

(38) Zhang, Z.; Yu, Z.-M.; Liu, G.-B.; Yao, Y. MagneticTB: A package for tight-binding model of magnetic and non-magnetic materials. *Comput. Phys. Commun.* **2022**, *270*, 108153.

(39) Liu, G.-B.; Shan, W.-Y.; Yao, Y.; Yao, W.; Xiao, D. Three-band tight-binding model for monolayers of group-VIB transition metal dichalcogenides. *Phys. Rev. B* **2013**, *88*, 085433.

(40) Cui, C.; Han, Y.; Zhang, T.-T.; Yu, Z.-M.; Yao, Y. Four-band tight-binding model of TiSiCO-family monolayers. *Phys. Rev. B* **2023**, *108*, 155115.

(41) Jain, A.; Ong, S. P.; Hautier, G.; Chen, W.; Richards, W. D.; Dacek, S.; Cholia, S.; Gunter, D.; Skinner, D.; Ceder, G.; Persson, A. j. K. Commentary: The Materials Project: A materials genome approach to accelerating materials innovation. *APL Mater.* **2013**, *1*, 011002.

(42) Curtarolo, S.; Setyawan, W.; Hart, G. L.; Jahnatek, M.; Chepulskii, R. V.; Taylor, R. H.; Wang, S.; Xue, J.; Yang, K.; Levy, O.; et al. AFLOW: An automatic framework for high-throughput materials discovery. *Comput. Mater. Sci.* **2012**, *58*, 218−226.

https://doi.org/10.1021/acs.nanolett.4c04527
Nano Lett. XXXX, XXX, XXX−XXX

(43) See Supporting Information for the detailed instructions of methods, FB systems, FCC TB model details, material details, *d* or *f* orbital details, and SC or BCC details.
(44) Zheng, Y.; Li, L.; Luo, N.; Tang, L.-M.; Feng, Y.; Chen, K.-Q.; Zhang, Z.; Zeng, J. Orbital-designed flat-band model and realization of superconductivity in three-dimensional materials. *Phys. Rev. B* **2024**, *109*, L180504.
(45) Hase, I.; Yanagisawa, T.; Aiura, Y.; Kawashima, K. Possibility of flat-band ferromagnetism in hole-doped pyrochlore oxides $Sn_2Nb_2O_7$ and $Sn_2Ta_2O_7$. *Phys. Rev. Lett.* **2018**, *120*, 196401.
(46) Ramachandran, A.; Andreanov, A.; Flach, S. Chiral flat bands: Existence, engineering, and stability. *Phys. Rev. B* **2017**, *96*, 161104.
(47) Wang, M.; Jiang, W.; Yao, Y. Three-dimensional flat band evolution between pyrochlore and perovskite lattices with enhanced anomalous Hall effect. *Phys. Rev. B* **2024**, *109*, 165147.
(48) Mostofi, A. A.; Yates, J. R.; Lee, Y.-S.; Souza, I.; Vanderbilt, D.; Marzari, N. wannier90: A tool for obtaining maximally-localised Wannier functions. *Comput. Phys. Commun.* **2008**, *178*, 685−699.
(49) Mostofi, A. A.; Yates, J. R.; Pizzi, G.; Lee, Y.-S.; Souza, I.; Vanderbilt, D.; Marzari, N. An updated version of wannier90: A tool for obtaining maximally-localised Wannier functions. *Comput. Phys. Commun.* **2014**, *185*, 2309−2310.
(50) Stoner, E. C. Collective electron ferromagnetism. *Proc. R. Soc. London Ser. A* **1938**, *165*, 372−414.
(51) Jiang, W.; Huang, H.; Liu, F. A Lieb-like lattice in a covalent-organic framework and its Stoner ferromagnetism. *Nat. Commun.* **2019**, *10*, 2207.

https://doi.org/10.1021/acs.nanolett.4c04527
Nano Lett. XXXX, XXX, XXX−XXX